Journal of Power Sources 240 (2013) 397–403

Contents lists available at SciVerse ScienceDirect

Journal of Power Sources

journal homepage: www.elsevier.com/locate/jpowsour

Nickel hydroxide electrode with porous nanotube arrays prepared by hydrolysis and cathodic deposition for high-performance supercapacitors

Mao-Sung Wu*, Jia-Fang Wu

Department of Chemical and Materials Engineering, National Kaohsiung University of Applied Sciences, Kaohsiung 807, Taiwan

HIGHLIGHTS

- Porous $Ni(OH)_2$ nanotubes are grown on stainless steel substrate.
- The porous wall provides much more channels for electrolyte access.
- Interconnected network structure of wall allows for electron conduction.
- Porous $Ni(OH)_2$ nanotube electrode is capable of delivering high capacitance.

ARTICLE INFO

Article history:
Received 16 July 2012
Received in revised form
28 March 2013
Accepted 7 April 2013
Available online 18 April 2013

Keywords:
Nickel hydroxide
Hydrolysis
Cathodic deposition
Supercapacitors
Porous nanotubes

ABSTRACT

This paper describes a strategy for fabricating porous nanotube arrays and how the $Ni(OH)_2$ electrode composed of porous nanotubes exhibits better pseudocapacitive behavior compared to $Ni(OH)_2$-coated ZnO nanorod and $Ni(OH)_2$ film electrodes. $Ni(OH)_2$ electrode with porous nanotubes is fabricated by hydrolysis and cathodic deposition using electrodeposited ZnO nanorods as a template. The $Ni(OH)_2$ nanoflakes grow on the stainless steel substrate and around the ZnO nanorods during cathodic deposition. After the removal of the ZnO template, hollow nanotubes with porous walls of interconnected nanoflakes are formed. The porous nanotube structure facilitates easy electrolyte transport to the reaction sites and leads to a further increase in the specific capacitance of electrode. The specific capacitance of porous $Ni(OH)_2$ nanotube electrode reaches as high as 1581 F g^{-1}, which is much higher than that of $Ni(OH)_2$-coated ZnO nanorod (874 F g^{-1}) and compact $Ni(OH)_2$ film (569 F g^{-1}) electrodes at a discharge current density of 1 A g^{-1}.

1. Introduction

Supercapacitors have become an attractive power solution for an increasing number of applications because they can offer higher power density and longer cycle life than the conventional batteries. Among various pseudocapacitive materials based on metal oxides or hydroxides, porous nickel hydroxide materials have received much research attention due to their intriguing chemical and physical properties. The unique nature of porous structures allows nickel oxide/hydroxide materials to be used for a wide variety of applications, such as batteries (especially for nickel–cadmium, nickel–metal hydride, and nickel–hydrogen batteries), supercapacitors, and electrochromic devices. Both high surface area and large pore volume are of critical importance for supercapacitor application. To enhance these factors, many attempts have been made. For example, liquid crystal template and surfactant template methods have been used to fabricate the mesoporous nickel oxide/hydroxide materials [1–4]. Generally, the high power characteristic of supercapacitors is limited by the ion diffusion rate in the solid materials rather than in the liquid solution because of the extremely low solid-sate diffusion rates. Several efforts have been made to increase the power characteristics of supercapacitors by reducing the material dimensions down to the nanometer scale, which can significantly reduce the ion diffusion time.

It was previously reported that the pseudocapacitance behavior and performance of an electroactive material are controlled not only by the surface area, pore size, and pore volume, but also by the surface morphology [5]. Nickel oxide/hydroxide materials with nanoflake or nanoplatelet morphologies have been reported to exhibit short diffusion path, high surface area, and suitable pore size for application in electrode materials [6–9]. Supercapacitors are expected to deliver high powder density in a very short period of time. If the solid-sate

* Corresponding author. Fax: +886 9 3830674.
E-mail address: ms_wu@url.com.tw (M.-S. Wu).

0378-7753/$ – see front matter © 2013 Elsevier B.V. All rights reserved.
http://dx.doi.org/10.1016/j.jpowsour.2013.04.035

diffusion rate is improved by using the nano-scaled materials, the high rate capability of capacitors may be limited by the electrolyte diffusion in narrow interstitial channels within the electrodes. Therefore, macroporous structures, such as nanotube [10–12], hollow-sphere [13–18], and core–shell [19] structures are widely considered to be effective for application in high-performance supercapacitors. Macropore plays an important role in enhancing the electrochemical performance of nickel oxide/hydroxide electrodes, especially at the high-rate charge and discharge circumstances. An electrode with macropores allows fast charging and discharging without significant capacity loss [20–22].

Hollow-sphere materials, which are promising as effective electrode materials, are typically prepared via a colloidal template technique, which is an easy method used to tailor the size and shape of outside materials by using various templates [23]. With sphere templates, including those composed of polystyrene or silica spheres, the active electrode materials can be coated on the spheres to form a core–shell structure. The hollow-sphere materials can be readily obtained by removing the core materials by solvent or thermal decomposition. ZnO nanorod/amorphous metal oxide shell composites were prepared by electrochemical deposition of metal followed by heat-treatment at a higher temperature [24]. The hollow structure of metal oxides can be obtained by the removal of ZnO template. Recently, a sacrificial template-accelerated hydrolysis has been reported to fabricate the iron oxide nanotube arrays without the need to remove ZnO template [25]. ZnO nanorod arrays are chosen as the sacrificial templates that do not contribute to the component of final iron oxide nanotubes but can be simultaneously dissolved by the acid generated from the hydrolysis of Fe^{3+}. The dissolution of ZnO template may accelerate the hydrolysis of Fe^{3+}, which is of importance for initiating the formation of nanotubes [25].

In the present work, we propose the nickel hydroxide nanotube arrays composed of porous wall for supercapacitor application. Nickel hydroxide was coated on the ZnO nanorods by hydrolysis of Ni^{2+} and cathodic deposition. After removal of the ZnO nanorods, the porous nanotube electrode was obtained. A possible deposition mechanism used to explain the formation of porous nanotubes is discussed. The electrochemical performance of a nickel hydroxide electrode composed of porous nanotubes was studied. We expect that the tailored structure featuring porous hollow nanotubes may facilitate electrolyte transport within the electrode and may consequently enhance the pseudocapacitive behavior of the nickel hydroxide electrode.

2. Experimental section

The ZnO template composed of hexagonal nanorod arrays was deposited directly onto the stainless steel (SS) foil by applying a cathodic potential of −0.8 V versus a saturated Ag/AgCl electrode at 60 °C for 15 min. The cathodic deposition of ZnO template was carried out in a homemade three-compartment cell. A saturated Ag/AgCl electrode was used as the reference electrode and a platinum foil (2 cm × 2 cm) was the counter electrode. The plating solution was a mixture of 5 mM zinc nitrate and 50 mM potassium chloride and was stirred using a Teflon stir bar on a magnetic plate during the deposition process. Prior to cathodic deposition, SS foil was cut into pieces of 2 cm × 2 cm, which were then soaked in acetone and ultrasonically vibrated for 5 min to wash away any contaminants from their surface. De-ionized water was then used to rinse the SS foils in ultrasonic vibration for another 5 min. After deposition, the template was rinsed several times in de-ionized water, and then the template was dried at 150 °C for 30 min in air.

Nickel hydroxide films were electrodeposited directly onto the ZnO-coated SS substrate and bare SS substrate at room temperature for 3 min. The potential applied for cathodic deposition was set to −0.8 V versus a saturated calomel electrode. The deposition bath consisted of 0.1 M nickel nitrate and 0.1 M potassium nitrate. The plating solution was stirred by a Teflon stir bar on a magnetic hot plate during the deposition. After deposition, the nickel hydroxide-coated ZnO electrode was rinsed several times in de-ionized water and then immersed in 6 M sodium hydroxide solution for 60 min to remove the remnants of ZnO template. The resultant porous nickel hydroxide electrode was dried at 100 °C for 1 h in air. The weight of deposited nickel hydroxide was measured to be approximately 0.2 mg cm^{-2} by a microbalance (Mettler, XS105DU) with an accuracy of 0.01 mg. The weight of active material (nickel hydroxide) in each electrode was held almost the same by tuning the deposition time.

The surface morphology of the nickel hydroxide electrode was examined with a scanning electron microscope (SEM) with an accelerating voltage of 3 keV. The porous structure of the nickel hydroxide was identified by a transmission electron microscope (TEM) with an accelerating voltage of 200 keV. Samples were stripped from electrodes for TEM measurement. The electrochemical behavior of the nickel hydroxide electrode was determined by cyclic voltammetry and galvanostatic charge–discharge test in a three-electrode cell with a 1 M KOH electrolyte. A saturated Ag/AgCl electrode was used as the reference electrode and a platinum foil with dimensions of 2 cm × 2 cm as the counter electrode. The potential was cycled at a scan rate of 1 mV s^{-1} using a potentiostat (CH Instruments, CHI 608) in a potential range of 0–0.45 V. The electrode was charged at a current density of 1 A g^{-1} to a cut-off potential of 0.45 V. The fully charged electrode was discharged at various current densities to a cut-off potential of 0.0 V. AC impedance measurements were performed by means of a potentiostat (CH Instruments, CHI 608) coupled to a frequency response analyzer under an open-circuit condition. An AC perturbation amplitude of 10 mV versus the open-circuit potential was applied in a frequency range from 50 kHz to 0.1 Hz. All chemicals used in this work were of analytical grade and were used as received without further purification.

3. Results and discussion

Fig. 1 illustrates the formation process of porous $Ni(OH)_2$ nanotubes. When the ZnO nanorod arrays are immersed in the plating solution, the nickel ions prefer to adsorb on the walls of the hexagonal ZnO nanorods rather than adsorb on the top surface of

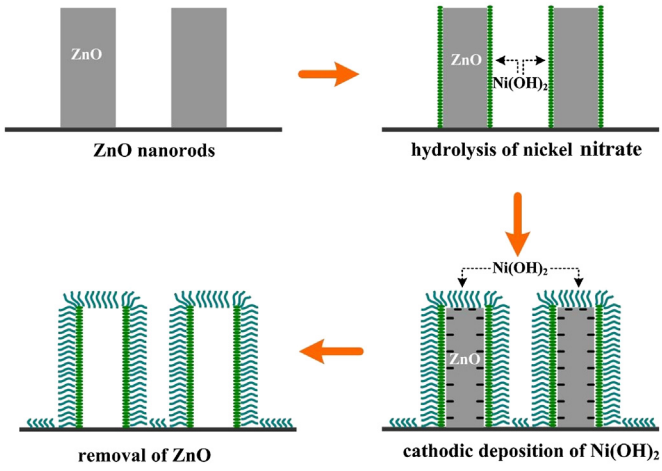

Fig. 1. Schematic illustrating the formation process of porous $Ni(OH)_2$ nanotubes.

the ZnO nanorods [11]. When the nickel ions are adsorbed on the ZnO surface, the hydrolysis of Ni^{2+} occurs simultaneously to form $Ni(OH)_2$ and H^+ as follows [25]:

$$Ni^{2+} + 2H_2O \rightarrow Ni(OH)_2 + 2H^+ \quad (1)$$

The ZnO nanorods are then etched by H^+. This etching reaction may accelerate the hydrolysis of Ni^{2+} [25]. Therefore, the unreacted ZnO core of the nanorods shrinks in size during the hydrolysis process. The $Ni(OH)_2$ grows in size until the ZnO core is entirely consumed. In this work, the hydrolysis time was limited to less than 1 min before cathodic deposition. Therefore, only a very small amount of ZnO wall can be etched during the hydrolysis of Ni^{2+}.

The cathodic deposition mechanism differs significantly from the hydrolysis of Ni^{2+}. $Ni(OH)_2$ nanoflakes can be coated on the exposed SS substrate and around the ZnO nanorods during cathodic deposition. The cathodic deposition of $Ni(OH)_2$ results from the chemical precipitation reaction between nickel ions and hydroxy ions. The generation of hydroxy ions may also be accompanied at the top surface of the ZnO nanorods, SS substrate, and the $Ni(OH)_2$-coated ZnO surface during the cathodic process in a nitrate-based electrolyte. The cathodic deposition mechanism can be expressed as follows:

$$NO_3^- + H_2O + 2e^- \rightarrow NO_2^- + 2OH^- \quad (2)$$

$$Ni^{2+} + 2OH^- \rightarrow Ni(OH)_2\downarrow \quad (3)$$

When a cathodic potential is applied, the positively charged nickel ions in the bulk electrolyte move to the negatively charged SS surface and react with the generated hydroxy ions, forming $Ni(OH)_2$ nanoflakes on the exposed SS surface. In addition, the $Ni(OH)_2$ film previously formed by hydrolysis of Ni^{2+} has an electrical conductivity that allows electron to be conducted from the bottom to the top of the $Ni(OH)_2$ deposits. In this case, $Ni(OH)_2$ grows around the ZnO nanorods, forming the $Ni(OH)_2$-coated ZnO nanorods. The hydrolysis of Ni^{2+} during the cathodic deposition may be mitigated by the neutralization reaction between H^+ and OH^- according to Equations (1) and (2). After deposition, the unreacted ZnO can be removed by etching with a concentrated sodium hydroxide solution because of the large difference in etching resistance between $Ni(OH)_2$ and ZnO in alkaline solution. Therefore, hollow nanotube composed of porous wall can be formed.

Fig. 2(a) shows the ZnO nanorods prepared by cathodic deposition method as the template for hydrolysis and cathodic deposition of porous $Ni(OH)_2$ nanotubes. The hexagonal ZnO nanorods have a diameter of about 86 nm and length of about 200 nm. The cathodic deposition of $Ni(OH)_2$ on the SS substrate has a film structure composed of nanoflakes shown in Fig. 2(b). SEM image of the $Ni(OH)_2$-coated ZnO nanorod arrays is shown in Fig. 2(c). ZnO nanorods have uniform $Ni(OH)_2$ wraps composed of interconnected nanoflakes. TEM images directly confirm the ZnO/$Ni(OH)_2$ core–shell structure in sample as shown in Fig. 3(a). The outer symmetric $Ni(OH)_2$ shell indicates the uniform wrap, which is about 23 nm in thickness. The unreacted ZnO core has a diameter of about 60 nm. EDS (Energy-dispersive X-ray spectroscopy) analysis showed that the ZnO content in the ZnO/$Ni(OH)_2$ core–shell composite was approximately 85 wt.%. The unreacted ZnO core may be etched completely by using a concentrated NaOH solution, forming the hollow tube structure with a macroscaled central channel (about 60 nm in diameter). After removal of ZnO core, the $Ni(OH)_2$ wall showed porous structure and was composed of interconnected nanoflakes shown in Fig. 3(b). A top-view TEM image shown in the inset of Fig. 3(b) reveals the hollow nanotube structure. The constituent $Ni(OH)_2$ nanoflakes in a porous nanotube remain interconnected as a network of electron-conducting

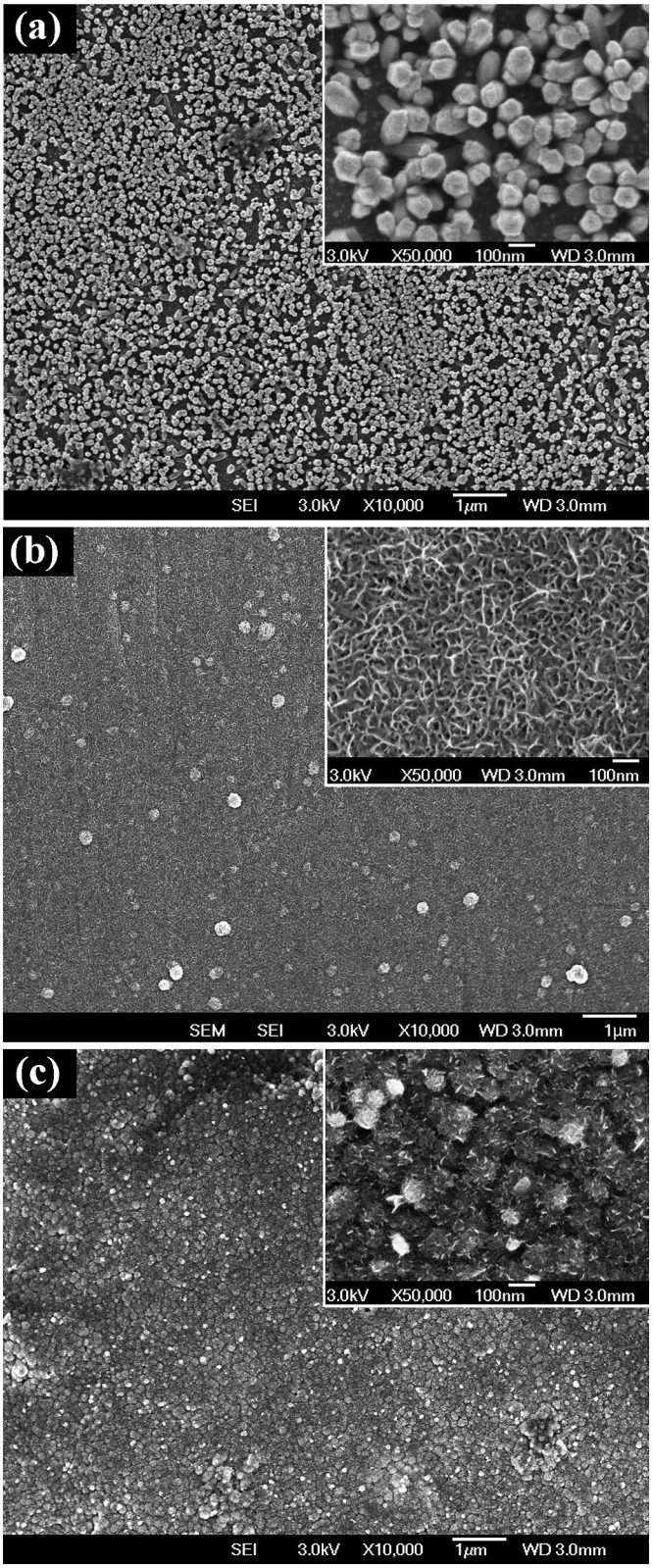

Fig. 2. SEM images of (a) ZnO nanorod arrays, (b) $Ni(OH)_2$ film, and (c) $Ni(OH)_2$-coated ZnO nanorod arrays. Inset shows the high-magnification SEM image.

paths, and the meso- and macroscaled pores between nanoflakes are easily accessible to liquid electrolyte. The ZnO content in the porous $Ni(OH)_2$ nanorods measured from EDS was less than 1 wt.% after etching process.

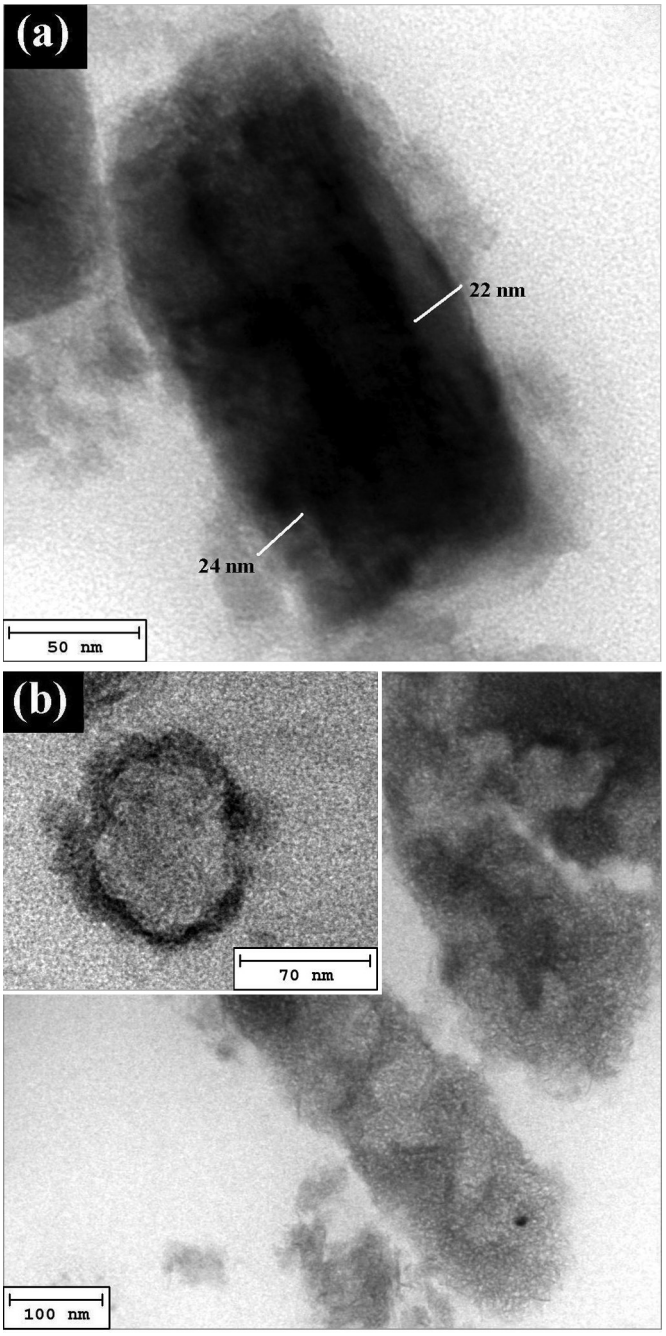

Fig. 3. TEM images of (a) $Ni(OH)_2$-coated ZnO nanorods and (b) porous $Ni(OH)_2$ nanotubes. Inset in (b) is a top-view TEM image of the porous $Ni(OH)_2$ nanotube.

As illustrated in Fig. 4, the $Ni(OH)_2$ electrode of spaced porous nanotube arrays can facilitate ion diffusion/migration and offer a large surface area in contact with the electrolyte. The electrolyte penetration through porous wall may occur. Therefore, the central channel of nanotube is filled with the electrolyte. The central region of nanotube exposed to electrolyte leads to a rapid motion of electrolyte along the tube axis. It was previously reported that the vertically aligned nanorods on conducting substrate provides much shorter paths for electron transport and the species diffusion thus improving their capacitive performance [26]. In this work, the interconnected network structure in porous $Ni(OH)_2$ wall provides a conduction path for electron, which is also an important factor that determines the electrochemical

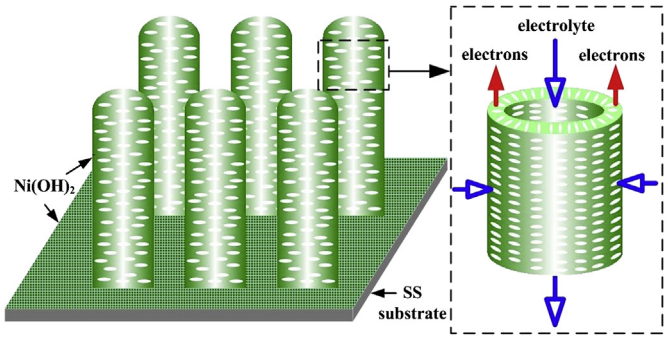

Fig. 4. Schematic illustrating the enhanced pseudocapacitive performance of $Ni(OH)_2$ electrode composed of porous nanotubes.

performances. The above advantages are very favorable for high electrochemical properties.

Fig. 5 shows the cyclic voltammograms (CVs) of porous $Ni(OH)_2$ nanotube, $Ni(OH)_2$ film, and $Ni(OH)_2$-coated ZnO nanorod electrodes. All electrodes show a couple of redox peaks due to the electrochemical reaction between $Ni(OH)_2$ and NiOOH in alkaline solution as follows [27]:

$$Ni(OH)_2 + OH^- \leftrightarrow NiOOH + H_2O + e^- \quad (4)$$

The oxidation and reduction peaks of both $Ni(OH)_2$ electrodes were observed at 0.40 V and 0.32 V, respectively. Through the faradaic (redox) reactions, higher capacitance can be stored in the bulk $Ni(OH)_2$ than at the electrolyte/electrode interface (electrical double layer). The $Ni(OH)_2$ electrode with porous nanotubes exhibited a higher current density than the $Ni(OH)_2$-coated ZnO nanorod and $Ni(OH)_2$ film electrodes, as revealed by the CV curves. CV curve of ZnO nanorod electrode in 1 M KOH aqueous solution, which is not shown here, was scanned for comparison. The current density of ZnO nanorod electrode is extremely low compared with that of $Ni(OH)_2$-coated ZnO nanorod electrode. Conclusively, current density of $Ni(OH)_2$-coated ZnO nanorod electrode comes mainly from the $Ni(OH)_2$ rather than the ZnO. The current density of $Ni(OH)_2$-coated ZnO nanorod electrode is based on the weight of the $Ni(OH)_2$ material. The higher the current density is, the larger the specific capacitance of the electrode becomes. After removal of

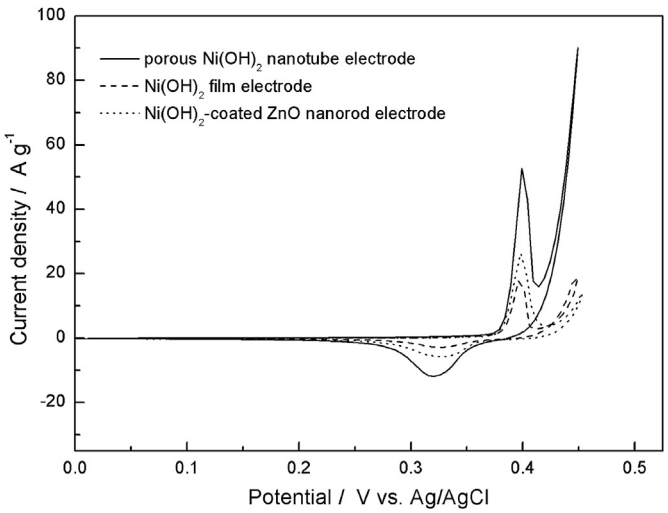

Fig. 5. CVs of porous $Ni(OH)_2$ nanotube, $Ni(OH)_2$ film, and $Ni(OH)_2$-coated ZnO nanorod electrodes at a scan rate of 1 mV s^{-1}.

the ZnO core, a porous $Ni(OH)_2$ wall composed of nanoflakes allows for the penetration of electrolyte into the hollow nanotubes. The large central channel of nanotubes facilitates the penetration of the electrolyte deep into the electrode, leading to a further increase in effective surface area for electrochemical reaction. The configuration of interconnected nanoflakes allows the electron conduction from the SS substrate to the top of nanotube. Therefore, the $Ni(OH)_2$ electrode composed of porous hollow nanotubes exhibited a higher current density than the $Ni(OH)_2$-coated ZnO nanorod and $Ni(OH)_2$ film electrodes during a potential sweep.

The specific capacitance value of the $Ni(OH)_2$ electrodes was measured by means of galvanostatic charge and discharge tests. Fig. 6 shows the discharging curves of the porous $Ni(OH)_2$ nanotube, $Ni(OH)_2$ film, and $Ni(OH)_2$-coated ZnO nanorod electrodes at a discharge current density of 1 A g^{-1}. The specific capacitance (C) of the $Ni(OH)_2$ electrodes during galvanostatic testing is calculated according to the equation:

$$C = \frac{i\Delta t}{\Delta V} \tag{5}$$

where i is the discharge current density (A g^{-1}), ΔV is the potential sweep window (V), and Δt is the discharge time (s). At a discharge current density of 1 A g^{-1}, the specific capacitance values of $Ni(OH)_2$ film, $Ni(OH)_2$-coated ZnO nanorod, and porous $Ni(OH)_2$ nanotube electrodes were measured to be approximately 569, 874, and 1581 F g^{-1}, respectively. The electrode with spaced nanorods gives greater surface area accessible to electrolyte ions than compact film electrode. Therefore, the $Ni(OH)_2$-coated ZnO nanorod electrode has a higher specific capacitance than the $Ni(OH)_2$ film electrode. The $Ni(OH)_2$ electrode with porous hollow nanotubes is capable of delivering a much higher specific capacitance than the $Ni(OH)_2$-coated ZnO nanorod and $Ni(OH)_2$ film electrodes. This suggests that the porous nanotube structure can enhance the performance of the electrode because of improved electrolyte transport through both the inner and outer nanotubes. The porous wall with network nanoflakes enable the unobstructed transportation of electrolyte ions and the conduction of electrons, leading to a very high specific capacitance of 1581 F g^{-1} at a discharge current density of 1 A g^{-1}.

The capacitance retention of an electrode under a high discharge rate is a noticeable factor for achieving practical application in batteries and capacitors because of the high power demand from portable electronic power tools and electric vehicles. Generally, an electrode has a lower capacitance when the discharge current density is high as a result of the faradaic reaction and ion diffusion resistances. Conventional capacitor suffers from poor power density at high-rate charge and discharge circumstances due to the presence of micropores in the electrode materials which are not easily accessible to electrolyte in a short period of time. The solution to this problem is to use macropores in the electrode materials. Fig. 7 shows the specific capacitance values of the $Ni(OH)_2$ electrodes at various discharge current densities. All electrodes have higher specific capacitance values at low current density than those at high current density. A $Ni(OH)_2$ electrode with porous nanotubes exhibits superior capacitance retention (95.2%) compared to $Ni(OH)_2$-coated ZnO nanorod (64%) and $Ni(OH)_2$ film (74%) electrodes at a high discharge current density of 10 A g^{-1}. The poor high-rate capability of $Ni(OH)_2$-coated ZnO nanorod electrode results from the low electrical conductivity of ZnO material. The high-rate performance of ZnO/$Ni(OH)_2$ core–shell electrode can be improved by removing the ZnO cores. A very small decrease in specific capacitance value with increasing discharge rate reveals the high power characteristics of a $Ni(OH)_2$ electrode with porous nanotubes. High capacitance retention at a high discharge rate also indicates that the faradaic reaction occurring on the active sites of $Ni(OH)_2$ surface is sufficiently fast. The novel structure of the porous hollow nanotubes with interconnected nanoflakes provides many more pore channels for electrolyte transport and conducting paths for electron, and the flake-like structure shortens the ion diffusion paths within the bulk of solid $Ni(OH)_2$. Thus, the capacitive behavior of a $Ni(OH)_2$ electrode with porous hollow nanotubes is significantly improved, particularly at high discharging rates.

Fig. 8 displays the Nyquist plots of porous $Ni(OH)_2$ nanotube, $Ni(OH)_2$ film, and $Ni(OH)_2$-coated ZnO nanorod electrodes. The intercept of the plots on the Z' axis at high frequencies is a combined resistance (R_s) of ionic resistance in electrolyte and intrinsic resistance of electrode materials. In this work, variations in R_s may result only from the intrinsic resistance of electrode materials, due to the same electrolyte used. R_s values for the porous $Ni(OH)_2$ nanotube, $Ni(OH)_2$ film, and $Ni(OH)_2$-coated ZnO nanorod electrodes were measured to be 0.4, 0.5, and 1.2 Ω, respectively. Clearly, the electrical conductivity of porous $Ni(OH)_2$ nanotube electrode is significantly improved by removing the ZnO nanorods. The semicircle in the high-frequency region corresponds to the charge-transfer resistance caused by the faradaic reaction and the double-layer capacitance on the $Ni(OH)_2$ surface. Apparently, the charge-transfer

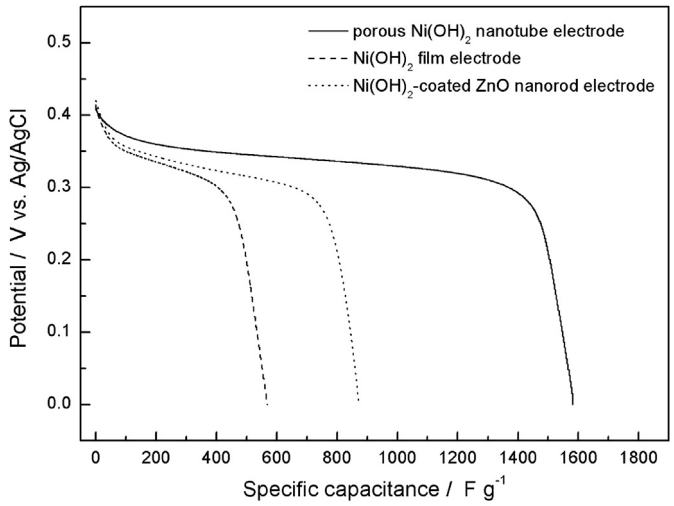

Fig. 6. Discharging curves of the porous $Ni(OH)_2$ nanotube, $Ni(OH)_2$ film, and $Ni(OH)_2$-coated ZnO nanorod electrodes at a discharge current density of 1 A g^{-1}.

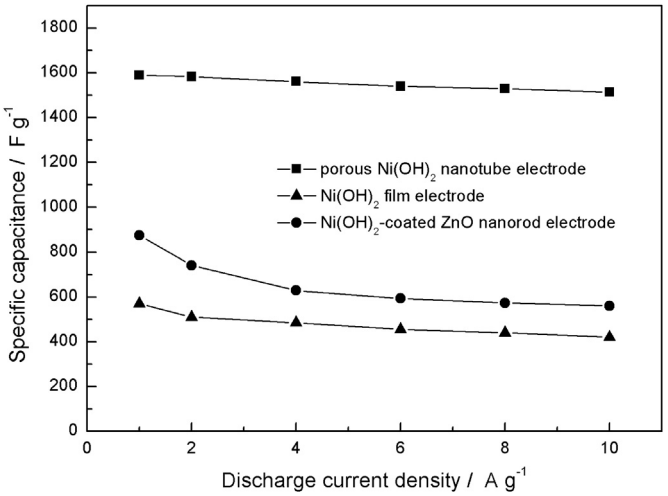

Fig. 7. Specific capacitances of the porous $Ni(OH)_2$ nanotube, $Ni(OH)_2$ film, and $Ni(OH)_2$-coated ZnO nanorod electrodes at various discharge current densities.

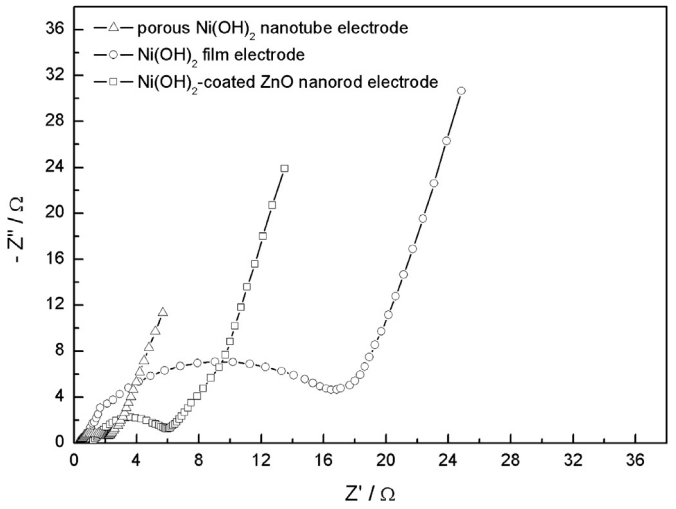

Fig. 8. Nyquist plots of the porous $Ni(OH)_2$ nanotube, $Ni(OH)_2$ film, and $Ni(OH)_2$-coated ZnO nanorod electrodes.

resistance of $Ni(OH)_2$ nanotube electrode is much lower than that of $Ni(OH)_2$-coated ZnO and $Ni(OH)_2$ film electrodes. Generally, the charge-transfer resistance is correlated with the number of active sites on the $Ni(OH)_2$ surface. In porous hollow nanotubes, the electrolyte could penetrate into the interior region of the $Ni(OH)_2$ matrix, leading to an increased number of active sites. The charge-transfer resistance was correspondingly reduced in the electrode composed of porous nanotube arrays. A comparison between porous $Ni(OH)_2$ nanotube and $Ni(OH)_2$-coated ZnO nanorod electrodes indicated that the presence of ZnO cores decreases the electrical conductivity of $Ni(OH)_2$-coated ZnO electrode and impedes the electrolyte transport through the inner nanotubes. The $Ni(OH)_2$ electrode with more compact film showed a relatively high charge-transfer resistance, reflecting that the specific capacitance primarily originates from the electrode surface, rather than the inner layer of the electrode. R_s value of the $Ni(OH)_2$ film electrode is slightly higher than that of porous $Ni(OH)_2$ nanotube electrode. Therefore, compared with $Ni(OH)_2$ film electrode, the improved capacitive behavior of porous $Ni(OH)_2$ nanotube electrode could be primarily attributed to the enhanced electrolyte transport within the electrode rather than the improved electron conduction. This result coincides with the high-rate electrochemical performance, the $Ni(OH)_2$ electrode of porous hollow nanotubes has a very small capacitance loss during high discharge current compared to the $Ni(OH)_2$ film and $Ni(OH)_2$-coated ZnO nanorod electrodes.

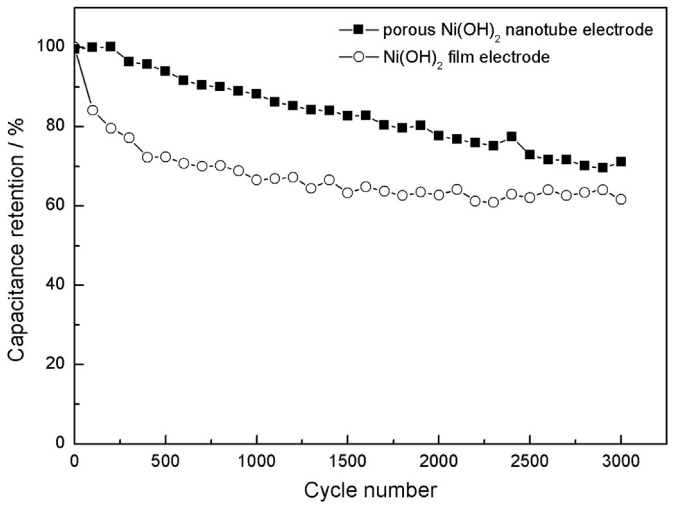

Fig. 9. Relationship between capacitance retention and cycle number for porous $Ni(OH)_2$ nanotube and $Ni(OH)_2$ film electrodes.

The electrode materials used in electrochemical capacitors and batteries are expected to have long cycle life. In this study, the cycle-life stability of $Ni(OH)_2$ electrodes was carried out by galvanostatic charging/discharging at 10 A g^{-1} for 3000 cycles. Fig. 9 shows the relationship between capacitance retention and cycle number for $Ni(OH)_2$ electrodes. The capacitance retention of both electrodes decreases slightly with increasing numbers of charging/discharging cycles. It was previously reported that the capacitance loss of $Ni(OH)_2$ during successive charging and discharging cycles is attributed to the oxygen evolution reaction, which can be improved by modifying the surface of the $Ni(OH)_2$ electrode with cobalt or cobalt oxide [28,29]. Both electrodes have similar capacitance retention after 3000 cycles, suggesting that the porous nanotube structure has no significant effect on the cycle-life stability of $Ni(OH)_2$ electrode.

4. Conclusions

When the ZnO nanorod arrays are immersed in the plating solution, the hydrolysis of Ni^{2+} occurs simultaneously to form $Ni(OH)_2$ deposits and H^+. The ZnO nanorods are etched by H^+. This etching reaction may accelerate the hydrolysis of Ni^{2+}. In this work, only a very small amount of ZnO wall can be etched by the hydrolysis of Ni^{2+} due to the limited hydrolysis time (less than 1 min). During cathodic deposition, nickel ions migrate close to the negatively charged electrode and react with the hydroxy ions generated by the electrochemical reduction of nitrate ions at the electrolyte/electrode interface, forming $Ni(OH)_2$ film on the exposed SS surface and around the ZnO nanorods. The SEM and TEM results indicated that the $Ni(OH)_2$ electrode with porous hollow nanotubes could be readily fabricated by hydrolysis and cathodic deposition processes using electrodeposited ZnO nanorods as a template. The pseudocapacitive behavior of porous $Ni(OH)_2$ nanotube electrode was investigated and compared with that of $Ni(OH)_2$-coated nanorod and $Ni(OH)_2$ film electrodes. The porous $Ni(OH)_2$ nanotube electrode exhibited a higher specific capacitance than the $Ni(OH)_2$-coated nanorod and $Ni(OH)_2$ film electrodes because the porous nanotube structure can offer a larger surface area for electrolyte access, leading to an enhancement in the performance of the $Ni(OH)_2$ electrode. Compared with film and nanorod electrodes, the porous nanotube is better in terms of increasing the effective surface area because the inner and outer surfaces of nanotubes are both in contact with the reaction medium. In this case, each porous hollow nanotube allows fast ion transport between the electrolyte and the electrode. In addition, the porous walls were composed of interconnected nanoflakes which offer conducting paths for electrons. Thus, the pseudocapacitive behavior of $Ni(OH)_2$ electrode with porous hollow nanotubes was considerably improved, particularly at high discharge rates. Therefore, the controlled hydrolysis and cathodic deposition of $Ni(OH)_2$ electrode is an effective approach to reduce transport limitations in the electrolyte.

Acknowledgments

The authors acknowledge financial support from the National Science Council, Taiwan (Project No: NSC101-2221-E-151-055-MY2).

References

[1] D.-D. Zhao, M.W. Xu, W.-J. Zhou, J. Zhang, H.L. Li, Electrochim. Acta 53 (2008) 2699–2705.

[2] B. Li, M. Ai, Z. Xu, Chem. Commun. 46 (2010) 6267–6269.
[3] D. Zhao, W. Zhou, H. Li, Chem. Mater. 19 (2007) 3882–3891.
[4] W. Xing, F. Li, Z.-F. Yan, G.Q. Lu, J. Power Sources 134 (2004) 324–330.
[5] S.K. Meher, P. Justin, G. Ranga Rao, Nanoscale 3 (2011) 683–692.
[6] J.-W. Lang, L.-B. Kong, W.-J. Wu, Y.-C. Luo, L. Kang, Chem. Commun. (2008) 4213–4215.
[7] H. Jiang, T. Zhao, C. Li, J. Ma, J. Mater. Chem. 21 (2011) 3818–3823.
[8] J. Liu, C. Cheng, W. Zhou, H. Li, H.J. Fan, Chem. Commun. 47 (2011) 3436–3438.
[9] H. Wang, H.S. Casalongue, Y. Liang, H. Dai, J. Am. Chem. Soc. 132 (2010) 7472–7477.
[10] X.-H. Li, L. Zhang, Z.-P. Bai, J.-J. Zhu, J. Nanosci. Nanotechnol. 10 (2010) 5191–5195.
[11] M.-S. Wu, K.-C. Huang, Chem. Commun. 47 (2011) 12122–12124.
[12] S. Xiong, C. Yuan, X. Zhang, Y. Qian, CrystEngComm 13 (2011) 626–632.
[13] G. Duan, W. Cai, Y. Luo, F. Sun, Adv. Funct. Mater. 17 (2007) 644–650.
[14] Y. Li, W. Li, S. Chou, J. Chen, J. Alloys Compd. 456 (2008) 339–343.
[15] C.-Y. Cao, W. Guo, Z.-M. Cui, W.-G. Song, W. Cai, J. Mater. Chem. 21 (2011) 3204–3209.
[16] S. Ding, T. Zhu, J.S. Chen, Z. Wang, C. Yuan, X.W. Lou, J. Mater. Chem. 21 (2011) 6602–6606.
[17] M.-S. Wu, K.-C. Huang, Int. J. Hydrogen Energy 36 (2011) 13407–13413.
[18] X.-H. Xia, J.-P. Tu, X.-L. Wang, C.-D. Gu, X.-B. Zhao, J. Mater. Chem. 21 (2011) 671–679.
[19] J.-H. Kim, S.H. Kang, K. Zhu, J.Y. Kim, N.R. Neale, A.J. Frank, Chem. Commun. 47 (2011) 5214–5216.
[20] M.-S. Wu, M.-J. Wang, Chem. Commun. 46 (2010) 6968–6970.
[21] D.-W. Wang, F. Li, H.-M. Cheng, J. Power Sources 185 (2008) 1563–1568.
[22] M.-S. Wu, M.-J. Wang, J.-J. Jow, J. Power Sources 195 (2010) 3950–3955.
[23] P.V. Braun, P. Wiltzius, Nature 402 (1999) 603–604.
[24] Y.-B. He, G.-R. Li, Z.-L. Wang, C.-Y. Su, Y.-X. Tong, Energy Environ. Sci. 4 (2011) 1288–1292.
[25] J. Liu, Y. Li, H. Fan, Z. Zhu, J. Jiang, R. Ding, Y. Hu, X. Huang, Chem. Mater. 22 (2009) 212–217.
[26] X. Lu, D. Zheng, T. Zhai, Z. Liu, Y. Huang, S. Xie, Y. Tong, Energy Environ. Sci. 4 (2011) 2915–2921.
[27] C.-C. Hu, C.-Y. Cheng, J. Power Sources 111 (2002) 137–144.
[28] X. Wang, H. Luo, H. Yang, P.J. Sebastian, S.A. Gamboa, Int. J. Hydrogen Energy 29 (2004) 967–972.
[29] Z. Chang, H. Li, H. Tang, X.Z. Yuan, H. Wang, Int. J. Hydrogen Energy 34 (2009) 2435–2439.